International Journal of Biological Macromolecules 109 (2018) 687–697

Contents lists available at ScienceDirect

International Journal of Biological Macromolecules

journal homepage: www.elsevier.com/locate/ijbiomac

# Carbon dots-modified chitosan based electrochemical biosensing platform for detection of vitamin D

Tamal Sarkar[a], H.B. Bohidar[b], Pratima R. Solanki[a,*]

[a] Special Centre for Nanoscience, Jawaharlal Nehru University, New Delhi, India
[b] School of Physical Sciences, Jawaharlal Nehru University, New Delhi, India

ARTICLE INFO

*Article history:*
Received 7 November 2017
Received in revised form
21 November 2017
Accepted 20 December 2017
Available online 21 December 2017

*Keywords:*
Chitosan
Carbon dots
Citric acid
Vitamin $D_2$
Electrochemical
Immunosenor

ABSTRACT

Here in, a carbon dots (CDs)-modified chitosan (CH) based biosensing platform was fabricated for vitamin $D_2$ detection. Carbon dots were synthesized through microwave pyrolysis method, and characterized with transmission electron microscopy, Raman spectroscopy, Fourier transform infrared spectroscopy, and UV/VIS spectroscopy. Chitosan (1%) solution was prepared in acetic acid (1%) solution and followed by the addition of CDs to prepare the carbon dots-chitosan (CD-CH) composite. A thin film of CD-CH composite was prepared onto ITO glass substrate (CD-CH/ITO) by drop casting method. Surface of the composite film was characterized by atomic force microscopy, static contact angle measurement and cyclic voltammetry. CD-CH/ITO surface was further modified with immobilization of vitamin $D_2$ antibody (Ab-$VD_2$) and bovine serum albumin (BSA) to prepare BSA/Ab-$VD_2$/CD-CH/ITO bioelectrode. Electrochemical response of the bioelectrode towards vitamin $D_2$ antigen (Ag-$VD_2$) was carried out by differential pulse voltammetry. The biosensing electrode showed linearity within the range 10–50 ng $mL^{-1}$ of Ag-$VD_2$ concentration. The sensitivity was found to be 0.2 μA $ng^{-1}$ mL $cm^{-2}$, LOD was 1.35 ng $mL^{-1}$, and the biosensor had a shelf-life of about 25 days.



## 1. Introduction

Carbon dots (CDs) are the new addition to the carbon nanomaterial family. CDs were accidentally discovered in 2004 while purifying and separating single-walled carbon nanotubes (SWCNT). Since its discovery CDs have attracted tremendous attention due to their electronic, biochemical, and optical properties [1] i.e., high solubility [2,3], green synthetic roots [2,4–6], stable fluorescence, easy functionalization, low toxicity [5], high electrochemical response, [7,8] and high biocompatibility [4]. Over the years, CDs have great potential for application in bioimaging [4,9], sensing [10–13], drug delivery [14], photoelectrochemistry [15] electrochemiluminescence [16,17], and optoelectronics [18–20]. There are various routes to synthesize CDs such as laser ablation [21], discharge method [22], combustion/thermal supported root [2,23,24], electrochemical oxidation root [25,26], and microwave pyrolysis method [14,16,27,28]. Among them, microwave pyrolysis method is more suitable, quick, cost-effective, and does not involve strong chemicals and produces high mass yield [3]. Zhaiet al., synthesized the CDs from citric acid (CA) and ethylenediamine (EDA) through microwave assisted pyrolysis. These CDs provided immense primary amine groups (—$NH_2$) along with carboxyl group (—COOH) on the surface of the CDs making them highly water soluble and suitable for biological application and other analysis [3,29]. The CDs are highly water soluble and are produced in very low yield for which it is very hard to form thin film/electrode for their application like electrode fabrication for electrochemical biosensing. There is a possibility that the incorporation of these CDs into a suitable matrix which can protect their properties for electrochemical application.

Chitosan is well known and suitable matrix for the dispersion of nanomaterials including CDs [30] for biosensor applications. Chitosan shows unique biological and chemical properties [31,32]. It has reactive hydroxyl and amino group, flexible for chemical modification, in its linear polyglucosamine chain [31,33,34]. Chitosan exhibits non-toxic, biocompatibility, biodegradability, and because of high mechanical strength biopolymer, it shows excellent film forming ability [35,36].The conductivity of chitosan can be improved by adding the conductive materials such as, carbon nanomaterials, metal nanoparticles, redox mediator and ionic liquid to form a relatively conductive film [37,38]. Huang et al., developed a biosensor to detect dopamine based on CDs-chitosan modified glassy carbon electrode (GCE) and detection limit obtained as 11.2 nM [39]. Further, they have achieved the lower detection limit up to 0.001 μM (1.0 nM) using nanocomposite comprising

* Corresponding author.
*E-mail address:* partima@mail.jnu.ac.in (P.R. Solanki).

https://doi.org/10.1016/j.ijbiomac.2017.12.122
0141-8130/

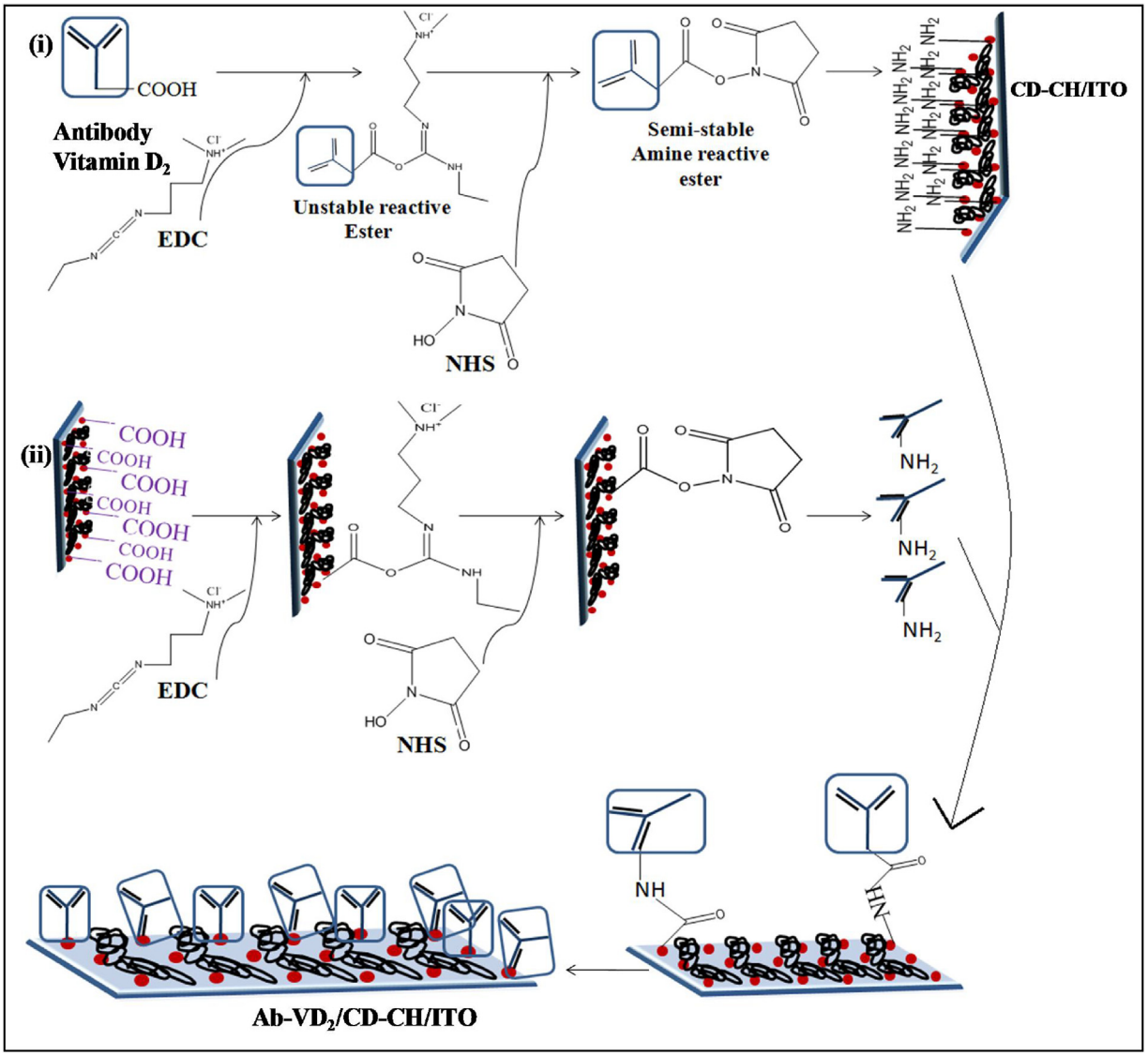


**Scheme 1.** Ab-$VD_2$ bonding with CD-CH/ITO electrode *via* EDC-NHS coupling; (i) EDC activated the carboxyl group of Ab-$VD_2$; (ii) EDC activated the carboxyl group of CDs.

of gold-CDs-chitosan modified GCE [40]. Sheng et al., prepared a film based on carbon nanodots and chitosan to entrap protein for direct electrochemistry [8]. However, carbon dots-chitosan (CD-CH) composite have a wide scope to explore for fabrication of immunosensor for vitamin D detection.

Vitamin D is essential for humans because it reduces the risk of common illness, infectious diseases, autoimmune diseases, and cardiovascular diseases [41]. Natural source of vitamin D is sunlight exposure, diet and dietary alternatives [42–44]. Vitamin D ($D_2$ and $D_3$), when taken through sunlight and diet, is metabolized in liver to 25 hydroxy vitamin D (25OHD) and in kidneys to 1,25 dihydroxy vitamin D [41,42,45]. Few foods sometimes are strengthened with vitamin D. Deficiency in vitamin D causes rickets as well as affects children and adults. During pregnancy in uterus and during childhood vitamin D deficiency can create skeletal deformation and growth retardation and may be a factor causing hip fracture in future life [41]. Also for adults, vitamin D deficiency can cause muscle weakness and osteoporosis may amplify the chance of fracture. Previously, few studies led to the understanding that vitamin $D_2$ is 30–50% less effective than vitamin $D_3$ for sustaining the serum 25-hydroxyvitamin D level [46,47]. Recently, Holick et al., proved that vitamin $D_2$ is equally significant as $D_3$ in maintaining the serum 25-hydroxyvitamin D in human [48]. Vitamin $D_2$ is obtained by ultra-violet irradiation of ergosterol of yeast. The conventional methods mainly to detect vitamin D are radioimmunoassay (RIA), HPLC–MS, and chemiluminescence [49,50]. These methods, having lengthy processes, require skill and high cost, making it hard for periodic use [51,52]. Chemiluminescence, although very suitable, built was not applied to detect vitamin $D_2$. Carlucci et al., designed a first biosensing platform based on gold nanoparticles (Au NPs) with 25OHD for vitamin D detection using electrochemical and surface plasmon resonance (SPR). They have reported that the electrochemical transducer exhibited the higher sensitivity with lower LOD value (10 ng/mL) [53]. As vitamin $D_2$ and $D_3$ both are equally significant to maintain the level of vitamin D, both vitamin $D_2$ and $D_3$ are equally important to be detected to know any kind deficiency of vitamin D. Thus, in this study bio-electrode was fabricated for the detection of vitamin $D_2$.

Here, a thin film of CD-CH was prepared by drop casting onto indium tin oxide (ITO) coated glass substrate for Vitamin $D_2$ detection using differential pulse voltammetry (DPV) technique. A specific antibody against the Vitamin $D_2$ (Ab-$VD_2$) and bovine serum albumin (BSA) were immobilized onto CD-CH/ITO film using EDC-NHS chemistry. This BSA/Ab-$VD_2$/CD-CH/ITO immunoelec-

trode exhibited the linear detection range of 1–50 ng $mL^{-1}$ of Ag $VD_2$.

## 2. Materials and methods

### 2.1. Reagents and solutions

Citric acid (CA) was purchased from SD Fine Chemical Ltd., India and ethylenediamine (EDA) from Alfa Aesar, Great Britain. Chitosan (CH) and 1-ethyl-3-(3-dimethylaminopropyl)-carbodiimide (EDC) was obtained from SRL, India. Polyclonal antibody against to Vitamin $D_2$ (Ab-$VD_2$) was procured from Cloud-Clone Corporation, USA and antigen as vitamin $D_2$ (Ag-$VD_2$) was ordered from Cayman Chemical, USA. Indium tin oxide (ITO) coated glass surface (Baltracom 247) was purchased from Balzers, UK. Bovine serum albumin (BSA), N-hydroxysuccinimide (NHS) was purchased from Sigma Aldrich, Germany. Potassium ferrocyanide ($K_4[Fe(CN)_6]$) and potassium ferricyanide ($K_3[Fe(CN)_6]$) were purchased from Fisher scientific chemical. Sodium chloride salt was purchased from SDFCL, India. Ethanol was procured from Merck, Germany.

### 2.2. Synthesis of carbon dots and CD-CH composite

For the synthesis of CDs, bottom up route was approached through microwave irradiation followed the procedure reported by Zhai et al. [3]. During the synthesis of CDs, 1gm CA was dissolved into 10 mL of distilled water. Then 50 μL EDA was added for enhanced carbonization. This clear colorless solution was baked into microwave (700 W) for 3 min. A red-brown thick solid foamy material was formed that allowed to cool down at room temperature and final volume made 5 mL with de-ionized water to dissolve. The resulting brown solution containing CDs and CA residue was dialyzed against water through dialysis membrane (MWCO 1000) for two days. A chitosan solution (1%) was prepared in acetic acid (1%) (10 mL). A CD-CH composite was prepared by mixing of 20 μL of prepared CDs into 10 mL chitosan solution (1%) under the vigorously stirred for 1 h.

### 2.3. Preparation of CD-CH/ITO electrode and functionalization with Ab-$VD_2$ and BSA

All the ITO coated glass substrates having same size (1.5 × 0.5 cm) were taken and then hydrolyzed. 30 μL of freshly prepared CD-CH solution was drop-casted onto hydrolyzed ITO glass substrate within an area of 0.25 $cm^2$ and dried in an oven at 60 °C, presented as CD-CH/ITO electrode. Similarly, CH solution (without CDs) was drop-casted onto ITO surface. A fresh solution of Ab-$VD_2$ (25 μg/L) was prepared into phosphate buffer saline (PBS, pH-7.4) containing 0.02% sodium azide. EDC (0.4 M) and NHS (0.1 M) solution was prepared in PB (pH-7). Ab-$VD_2$ was mixed with EDC (activator) and NHS (coupling agent) in the ratio of 2:1:1. During reaction time, EDC activated the carboxyl group of Ab-$VD_2$ and produced unstable O-acylisourea ester. This unstable ester reacted with NHS to form semi-stable amine reactive NHS ester. This NHS-activated Ab-$VD_2$ helped in crosslinking with amine groups of EDA present on the surface of CDs forming an amide bond [54]. Unreacted EDC could also activate carboxyl group present on the surface of CDs and form amide bond with one *Fab* region of Ab-$VD_2$ by diimide activated amidation process [55]. The two possibilities of AD-$VD_2$ binding were presented in graphical manner (Scheme 1).

20 μL of Ab-$VD_2$ solution (Scheme 1) was casted onto the CD-CH/ITO electrode and kept inside a humid chamber for 4 h at room temperature (25 °C). Ab-$VD_2$/CD-CH/ITO bioelectrode was rinsed with PBS to remove any unbounded antibody. Finally to block any non-specific active sites, BSA (10 μL of concentration 1 mg/mL) was dropped onto the bioelectrode and kept for 1 h. The BSA/Ab-$VD_2$/CD-CH/ITO bioelectrode was kept at 4 °C when not in use. Ag-$VD_2$ solutions were prepared in the range of 1–50 ng $mL^{-1}$ in ethanol by serial dilution method (Scheme 2).

### 2.4. Characterizations

The morphology and size of the CDs were characterized by high resolution transmission electron microscopy (HR-TEM, JEOL JEM-2200 FS, Japan). For TEM sample preparation, one drop of CDs suspension was casted on carbon coated copper grid. A Raman spectrum was recorded for CDs on EnSpectr R532. Absorbance was measured on T90+ UV/VIS spectrometer. A fluorescence characteristic of CDs was observed on Cary Eclipse Fluorescence spectrometer. The roughness of CD-CH/ITO and CH/ITO films were studied by atomic force microscopy (Park XE-70, Korea). The wettability of these electrodes was viewed using contact angle measurement SURFTENS universal (OEG GmbH Germany). Presence of antibody and BSA was also confirmed by infrared spectroscopy (Varian 7000 FT-IR instrument). The zeta potential was measured on an electrophoresis instrument (ZC-2000, Microtec, Japan). All electrochemical studies (cyclic voltammetry, differential pulse voltammetry and frequency response analysis) were done in Autolab Potentiostat/Galvanostat (Eco Chemie, Netherlands) in phosphate buffer saline (PBS, 0.2 M, pH −7.4) containing 5 mM $[Fe(CN)_6]^{3-/4-}$.

## 3. Results and discussions

### 3.1. Physical characterizations

Fig. 1A shows the TEM and HRTEM images of CDs. The CDs had spherical shaped structure with uniform distribution without apparent aggregation [Image (a)]. The size distribution of CDs was spread between the narrow range of 1.4-2.2 nm and average size found as 1.7 nm [inset Image 1(a)]. Image (b) shows the HRTEM image of the synthesized CDs, individual CD marked by white dotted line. HRTEM image revealed that the some CDs having crystalline in nature as shown in image (c), which justified the appearance of D and G bands in RAMAN spectra (Fig. 1B). It was revealed that the inter-planer spacing was 0.21 nm which corresponds to graphite [Image 1A(c)]. SAED pattern of CDs showed the ring formation of the planes of CDs [Image 1 (d)].

Raman spectrum of CDs shows D-band at 1352 $cm^{-1}$ and G-band at 1607 $cm^{-1}$ (Fig. 1B). The $I_D$ and $I_G$ are the area intensity corresponding to D-band and G-band, respectively. The ratio $I_D/I_G$ was found to be 1.38 which corresponds to $sp^3/sp^2$ carbon and the extent of disorder, implied that there were introduction of structural defects into the CDs after oxidation [56].

UV–vis absorption and PL luminescence were studied to evaluate the optical properties of CDs. The UV–vis spectrum [Fig. 1C(a)] showed a peak in UV region around 345 nm and tail stretching into visible region. This absorbance peak might correspond to π-π* transition of C=C bond [57]. The fascinating property of CDs was their excitation and size dependence PL luminescence behavior. The synthesized CDs showed blue luminescence under UV excitation [Fig. 1C(b)]. The intensity and the wavelength of emission are clearly dependent on excitation wavelength. CDs had a maximum emission at 360 nm. Excitation wavelength was varied from 320 to 420 nm. This excitation behavior of CDs could be explained by the presence of difference particle size and different emissive sites on the surface of CDs [58].

For the evidence of functional groups present, FTIR spectrum (Fig. 1D) were characterized. The broad absorption band near 3400 $cm^{-1}$ and peaks within the range of 1000–1300 $cm^{-1}$ corre-

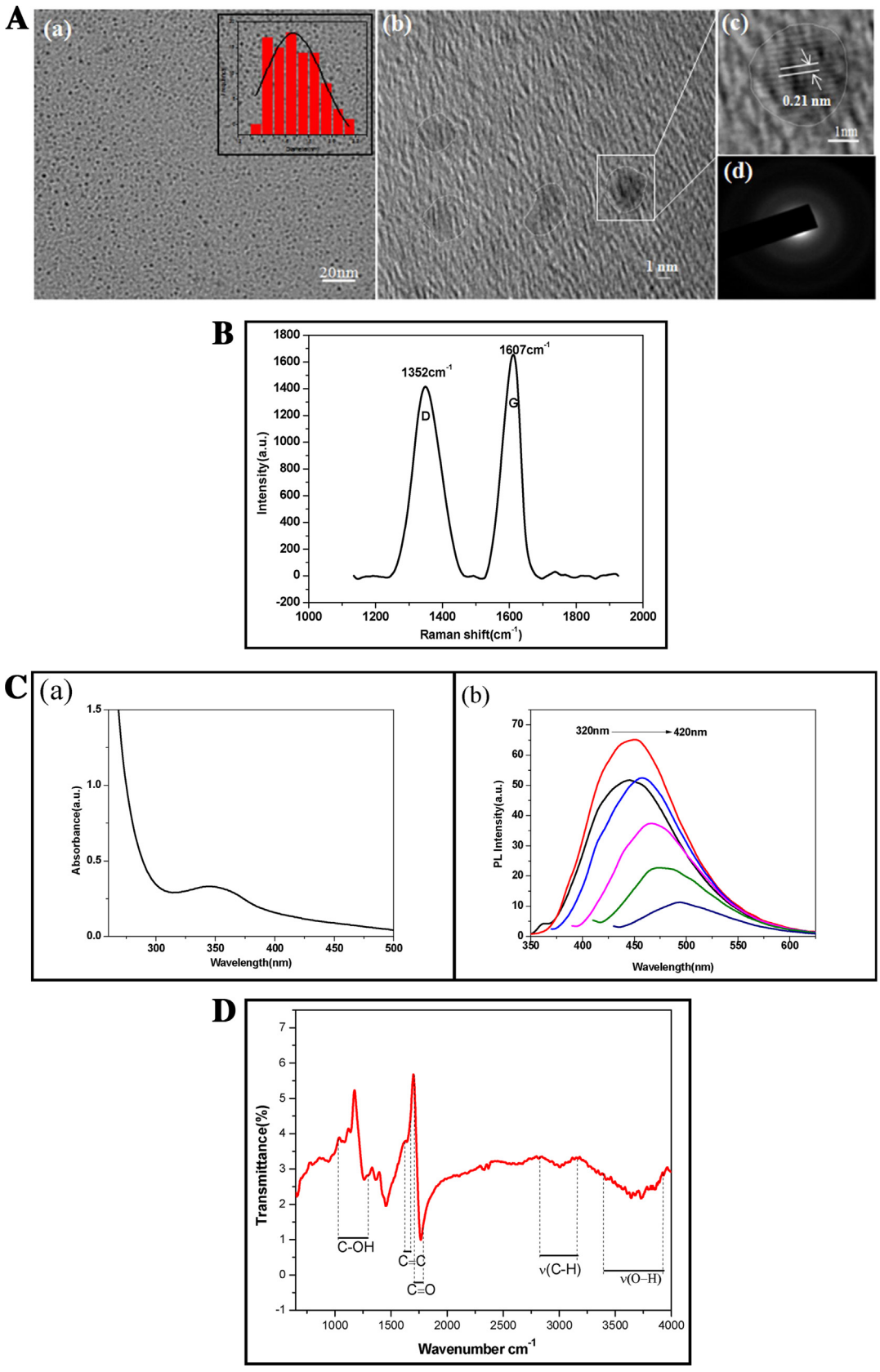


**Fig 1.** A: TEM study of CDs (a) uniformly distributed CDs of nearly spherical shape; (b) & (c) HRTEM image and inter-planer distance; (d) SAED pattern of CDs. B: Raman spectrum of CDs. C: OCptical properties (a) UV–vis absorption of CDs; (b) Photoluminescence spectra at different excitation wavelength (320–420 nm). D: FDTIR spectrum of CDs. E: AEFM study of (A) ITO, (B) CH/ITO, and (C) CD-CH/ITO electrodes; Roughness was seen in (a) topographic, (b) three dimensional and (c) cross sectional mode. F: Static contact angle of water drop making with (a) CH/ITO and (b) CD-CH/ITO electrodes.

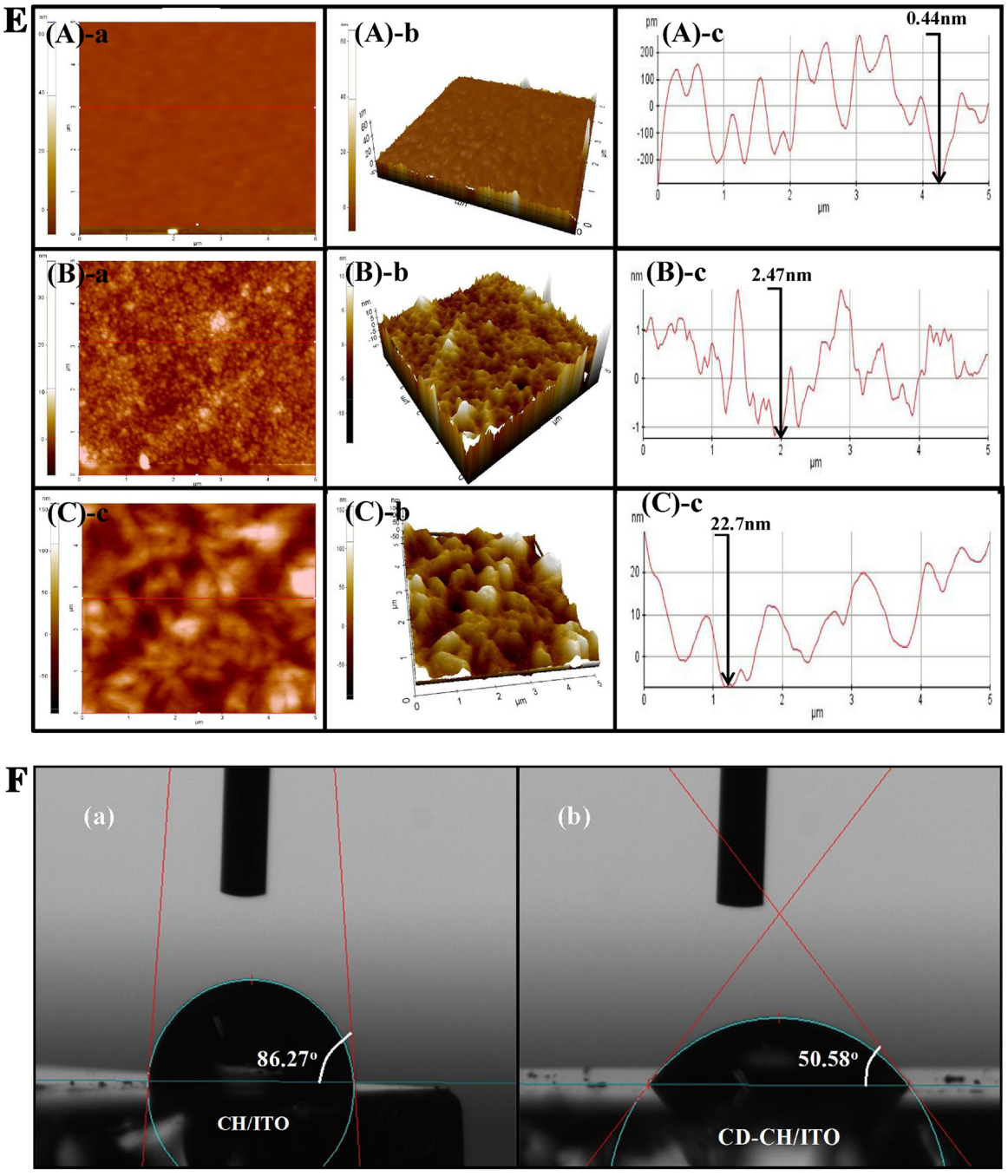


**Fig 1.** (*Continued*)

sponds to O—H bending vibration and C—OH stretching [3]. This confirmed the abundance of —COOH group. The availability of —COOH group supported by negative zeta potential (–20 mV) of CDs. Absorption band around 3000 $cm^{-1}$ could be due to C—H stretching and out of plane bending modes [59]. The IR peak around 1625 $cm^{-1}$ represents the characteristic peak for C=C stretching of CDs [60]. The very sharp peak appeared at 1760 $cm^{-1}$ could be assigned for C=O stretching. All these functional groups present in CDs confirmed the excellent hydrophillicity that provide a suitable support for immobilization of biomolecules.

The surface morphology of CH/ITO electrode and CD-CH/ITO electrode were characterized by AFM study. Fig. 1E shows topographic (a), three dimensional (b), and cross-sectional roughness of ITO (A), CH/ITO (B) and CD-CH/ITO (C) electrodes within an area of 5 μm×5 μm. The surface of bare ITO was very flat and smooth having largest peak height of 0.44 nm [Image (A)-a,b,c]. But CH/ITO surface exhibited a several adjacent peaks with an average peak height of 2.47 nm [Image (B)-a,b,c], which confirms the position of CH onto ITO glass substrate. However, after modification of CH with CDs the adjacent peak height differences increased with a higher average peak height of 22.7 nm [Image (C)-a,b,c]. Moreover, the average roughness (Ra) of ITO and CD/ITO surface were obtained to be 0.11 nm and 0.57 nm, respectively. The value of Ra of CD-CH/ITO electrode was found much higher (7.77 nm) as compared to CH/ITO electrode (0.57 nm). This increase in roughness confirmed the modification of CH by CDs. Modification of CH by CDs were not only improve the surface effect but also laid the ground for higher possibility of bio-functionalization.

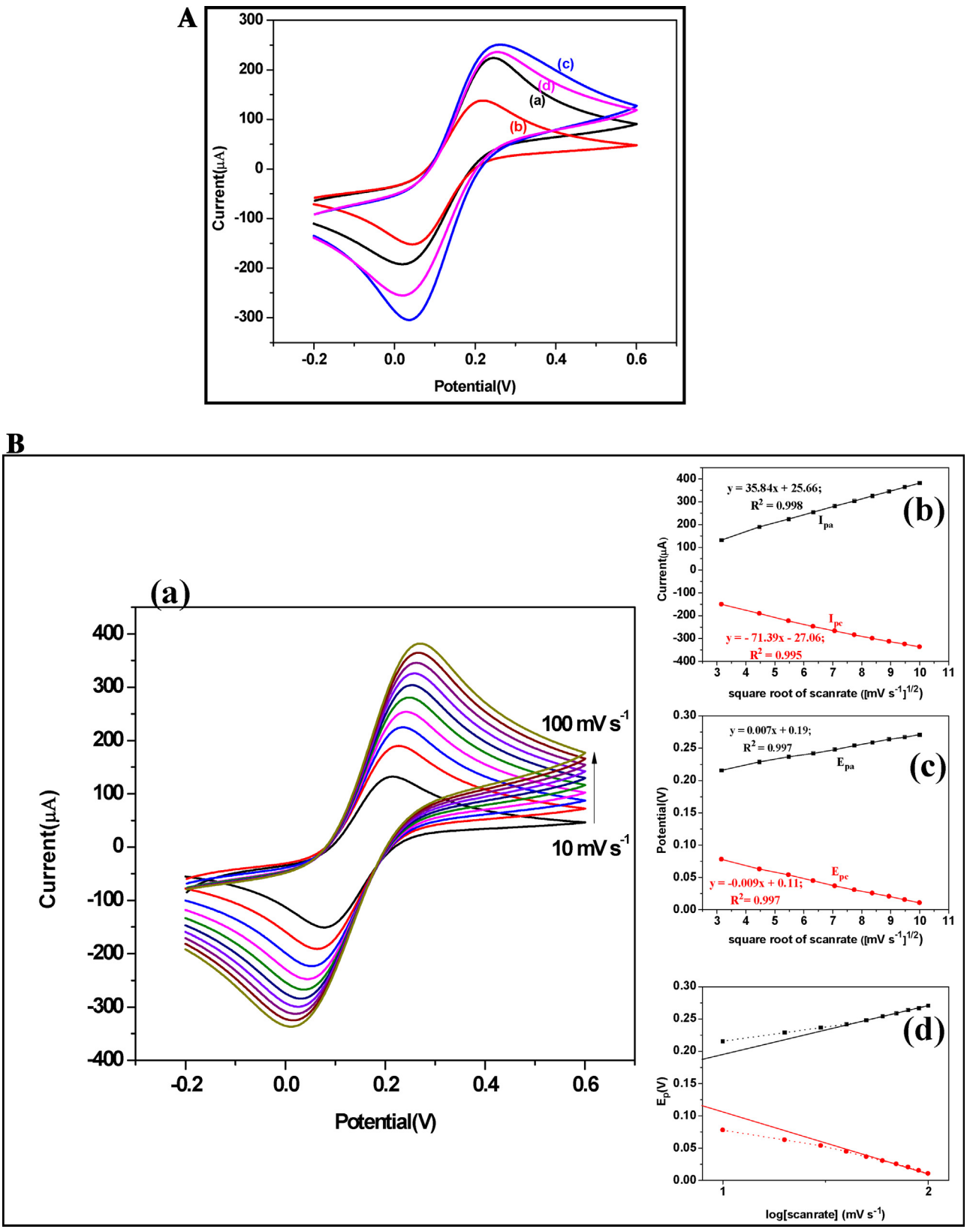


**Fig 2.** A: Cyclic voltammogram of (a) ITO, (b) CH/ITO, (c) CD-CH/ITO electrodes, and (d) BSA/Ab-$VD_2$/CD-CH/ITO bioelectrode in PBS containing $[Fe(CN)_6]^{3-/4-}$. B: (a) Cyclic voltammogram of BSA/Ab-$VD_2$/CD-CH/ITO bioelectrode in PBS containing $[Fe(CN)_6]^{3-/4-}$; (b) anodic ($I_{pa}$) and cathodic ($I_{pc}$) peak current with respect to square root of scan rate; (c) anodic ($E_{pa}$) and cathodic ($E_{pc}$) peak potential with respect to square root of scan rate; (d) anodic ($E_{pa}$) and cathodic ($E_{pc}$) peak potential with respect to logarithm of scan rate. (A) Frequency response analysis of (a) ITO, (b) CH/ITO, (c) CD-CH/ITO, electrode and (d) BSA/Ab-$VD_2$/CD-CH/ITO bioelectrode; (B) (i) Randles equivalent circuit and (ii) modified Randles equivalent circuit.

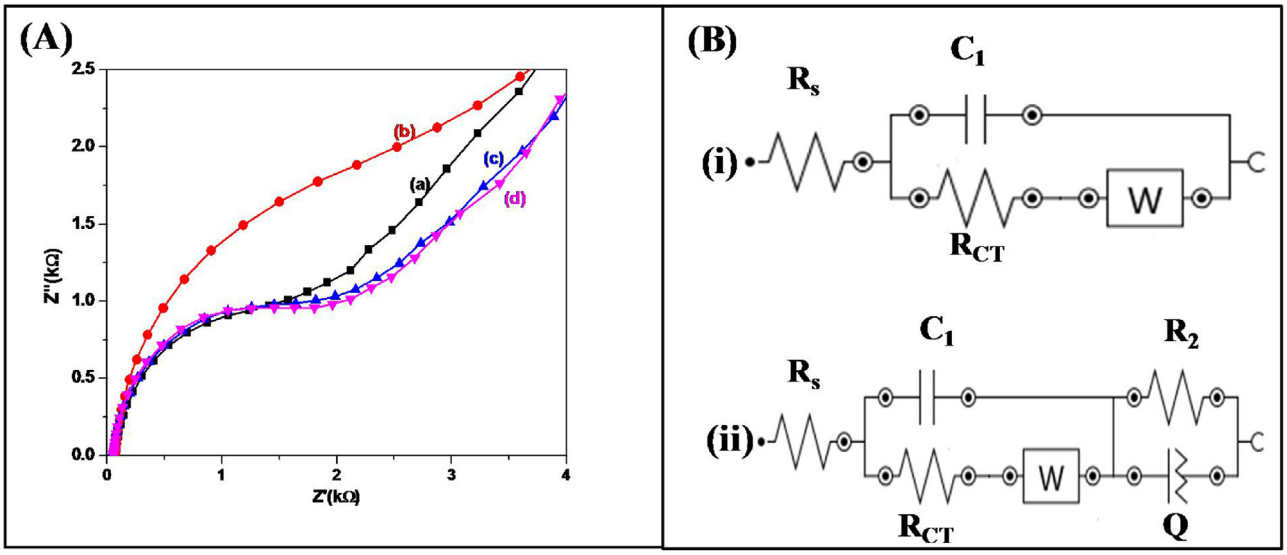


**Fig 2.** (*Continued*)

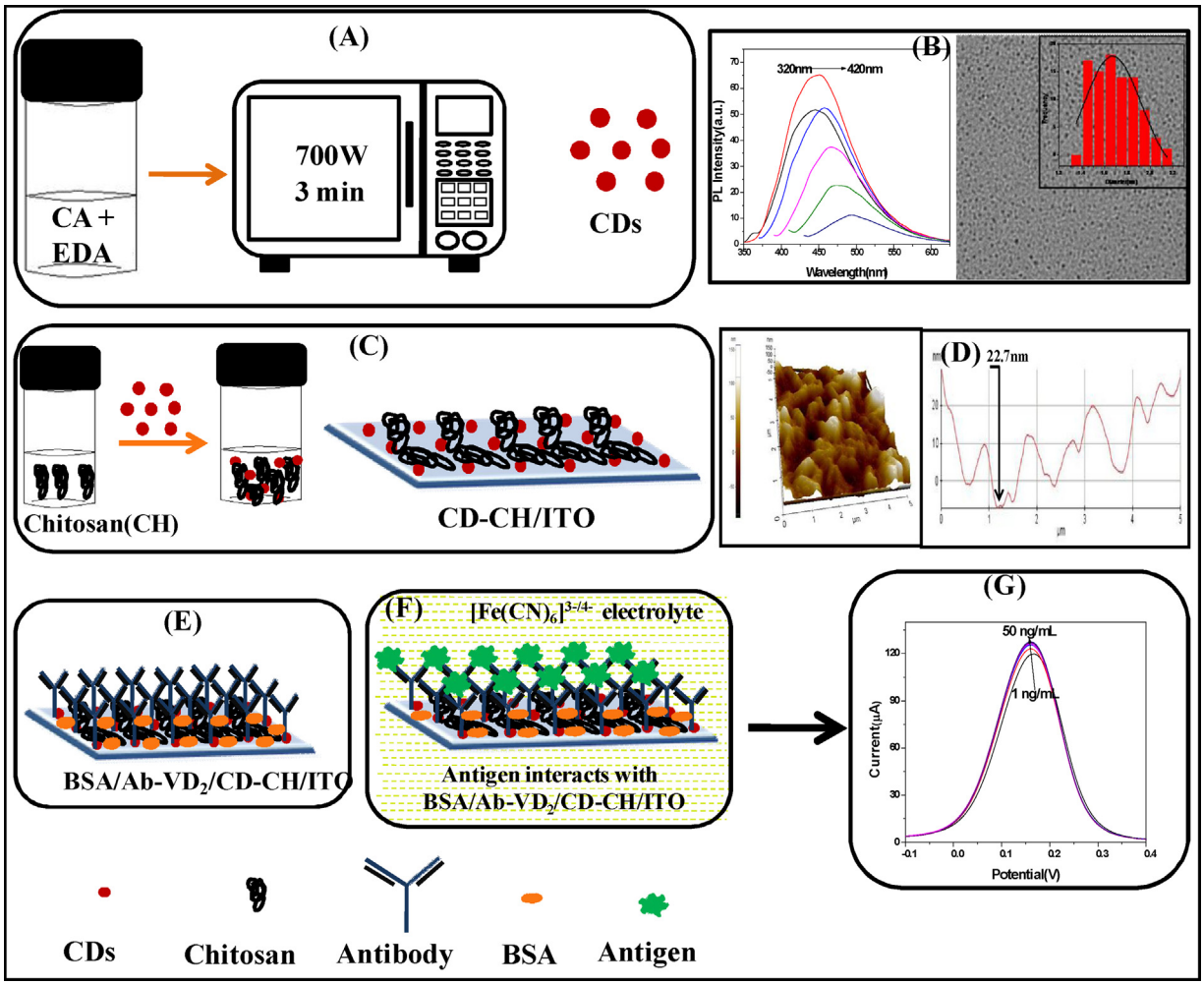


**Scheme 2.** (A) Synthesis of CDs; (B) PL spectra and TEM image of CDs; (C) composite film preparation; (D) AFM study of CD-CH/ITO electrode; (E) CD-CH/ITO electrode with Ab-$VD_2$ and BSA; (F) Interaction of $VD_2$ with BSA/Ab-$VD_2$/CD-CH/ITO in PBS containing $[Fe(CN)_6]^{3-/4-}$; (G) DPV response of the BSA/Ab-$VD_2$/CD-CH/ITO bioelectrode in presence of Ag-$VD_2$.

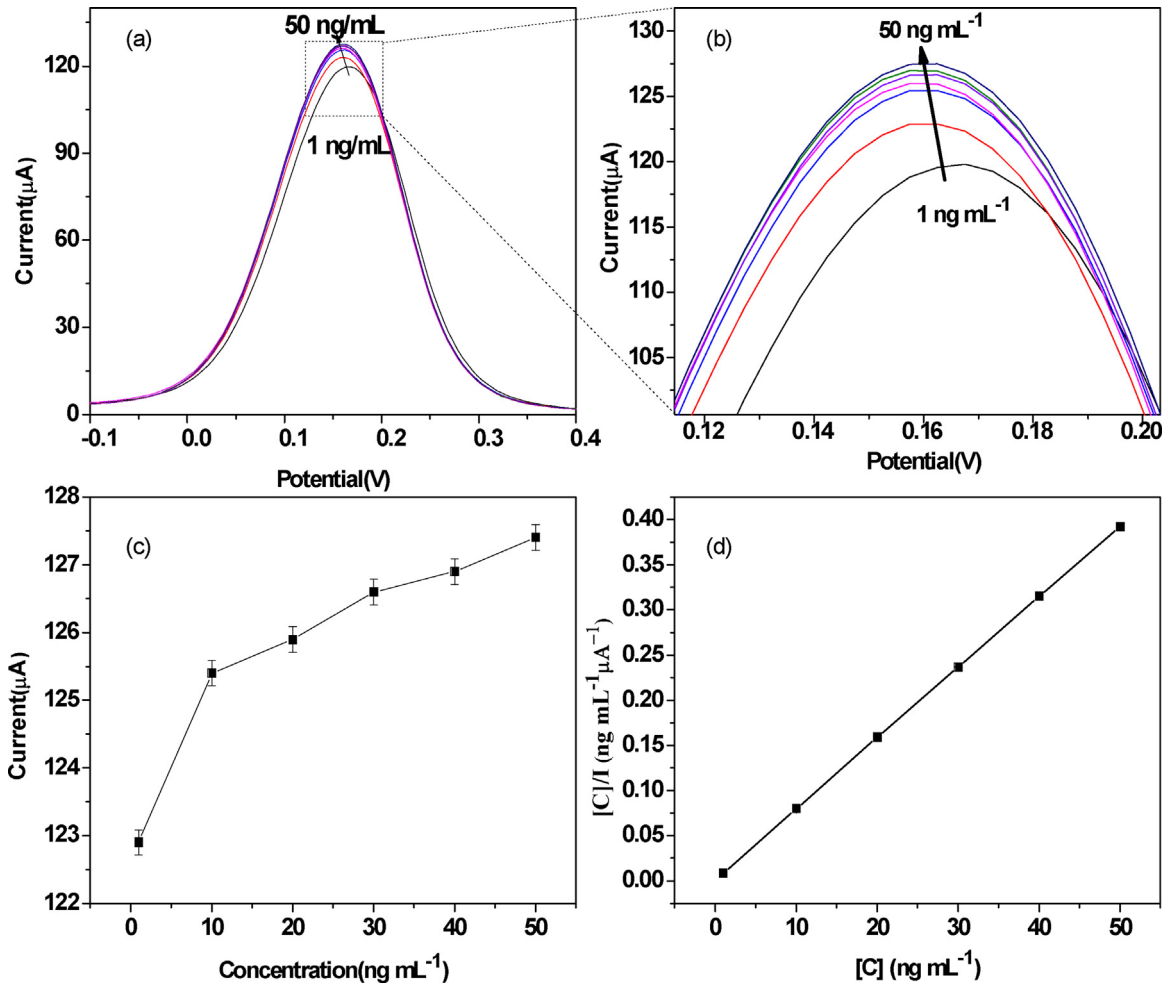


**Fig. 3.** Response study of BSA/Ab-$VD_2$/CD-CH/ITO bioelectrode with different conc. of Ag-$VD_2$; (a) DPV response with respect to conc. of Ag-$VD_2$(1–50 ng $mL^{-1}$); (b) amplified DPV response; (c) calibration plot of peak current vs conc. of Ag-$VD_2$; (d) Hanes Woolf Graph plotted between [*C*]/*I*vs [*C*], [*C*] be the conc. of Ag-$VD_2$.

Hydrophilicity and spread-ability/surface wettability of an electrode depends greatly on surface chemistry. As the effective charges stay on the electrode surface, wettablity of the surface is very significant. For that static contact angle measurement was performed for CH/ITO and CD-CH/ITO electrodes (Fig. 1F). A water droplet was produced over the respective electrode using a syringe, and static contact angle was measured at the interface of water and electrode surface. The static contact angle value for CH/ITO and CD-CH/ITO were obtained to be 86.27° (Image a) and 50.58° (Image b), respectively. Due to excess availability of carboxyl (—COOH) groups on the surface of CDs i.e., on CD-CH/ITO increased the hydrophilicity as compared to CH/ITO. It was also observed that (within a few second) the static contact angle decreased very rapidly in case of CD-CH/ITO electrode. However, in case of CD/ITO electrode, the surface got wrinkled within few second after treated with water droplet. Thus modification of electrode with CDs improved the hydrophilicity in great extent confirming suitable supports for interaction with antibodies prepared in PBS.

### 3.2. Electrochemical characterization

The electrochemical behavior of (a)ITO, (b) CH/ITO, (c) CD-CH/ITO and, (d) BSA/Ab-$VD_2$/CD-CH/ITO electrode were studied by cyclic voltammetry (CV) technique at 50 $mVs^{-1}$ scan rate in PBS containing $[Fe(CN)_6]^{3-/4-}$(Fig. 2A). The magnitude of current of CH/ITO electrode exhibited a distinct oxidation (0.23 V) and reduction (0.08 V) peak with maximum anodic peak current ($I_{pa}$) of 128 μA. After modification of CH with CDs, the $I_{pa}$ increased about three time (376 μA). This enhanced peak current due to free in carboxyl and amine group present enormously on the surface of CDs speed up the movement of electrons generated in electrolyte. After immobilization of Ab-$VD_2$ and BSA onto CD-CH/ITO electrode surface the electrochemical current decreased due to interaction of macromolecules sized Ab-$VD_2$ and BSA with freely available functional groups onto electrode surface. These results confirmed the modification of CD-CH/ITO electrode surface with Ab-$VD_2$ and BSA.

Cyclic voltammogram of BSA/Ab-$VD_2$/CD-CH/ITO bioelectrode was taken at 10–100 $mVs^{-1}$ scan rate in PBS (pH–7.4) containing $[Fe(CN)_6]^{3-/4-}$[Fig. 2B(a)] in a potential range −0.2V–0.6 V. The anodic ($I_{pa}$) and cathodic ($I_{pc}$) peak current was increased linearly with square root of scan rate which was an clear indication of quasi reversible or diffusion controlled oxidation and reduction. Also the anodic ($E_{pa}$) and cathodic ($E_{pc}$) peak potentials varied linearly with square root of scan rate [Fig. 2B(b-c)], indicating a friendly electron transfer kinetics. By linear fitting the values of slop, intercept and linear regression coefficient of linear behavior of peak currents and potentials were calculated (Eqs. (1)–(4)).

$$I_{pa} = 25.66\,\mu A + 35.84\,\mu A(mV\,s^{-1})^{-1/2} \times [scanrate]^{1/2}(mV\,s^{-1})^{1/2};\ R^2 = 0.998 \quad (1)$$

$$I_{pa} = -27.06\,\mu A - 71.39\,\mu A\,(mVs^{-1})^{-1/2} \times [scanrate]^{1/2}(mV\,s^{-1})^{1/2};\ R^2 = 0.995 \quad (2)$$

$$E_{pa} = 0.19\,V + 0.007\,V\,(mV\,s^{-1})^{-1/2} \times [scanrate]^{1/2}(mV\,s^{-1})^{1/2};\ R^2 = 0.997 \quad (3)$$

$$E_{pa} = 0.11\,V - 0.009\,V(mV\,s^{-1})^{-1/2} \times [scanrate]^{1/2}(mV\,s^{-1})^{1/2};\ R^2 = 0.997 \quad (4)$$

The anodic and cathodic peak potentials ($E_{pa}$, $E_{pc}$) were plotted against natural logarithm of scan rate [Fig. 2B(d)]. It was observed

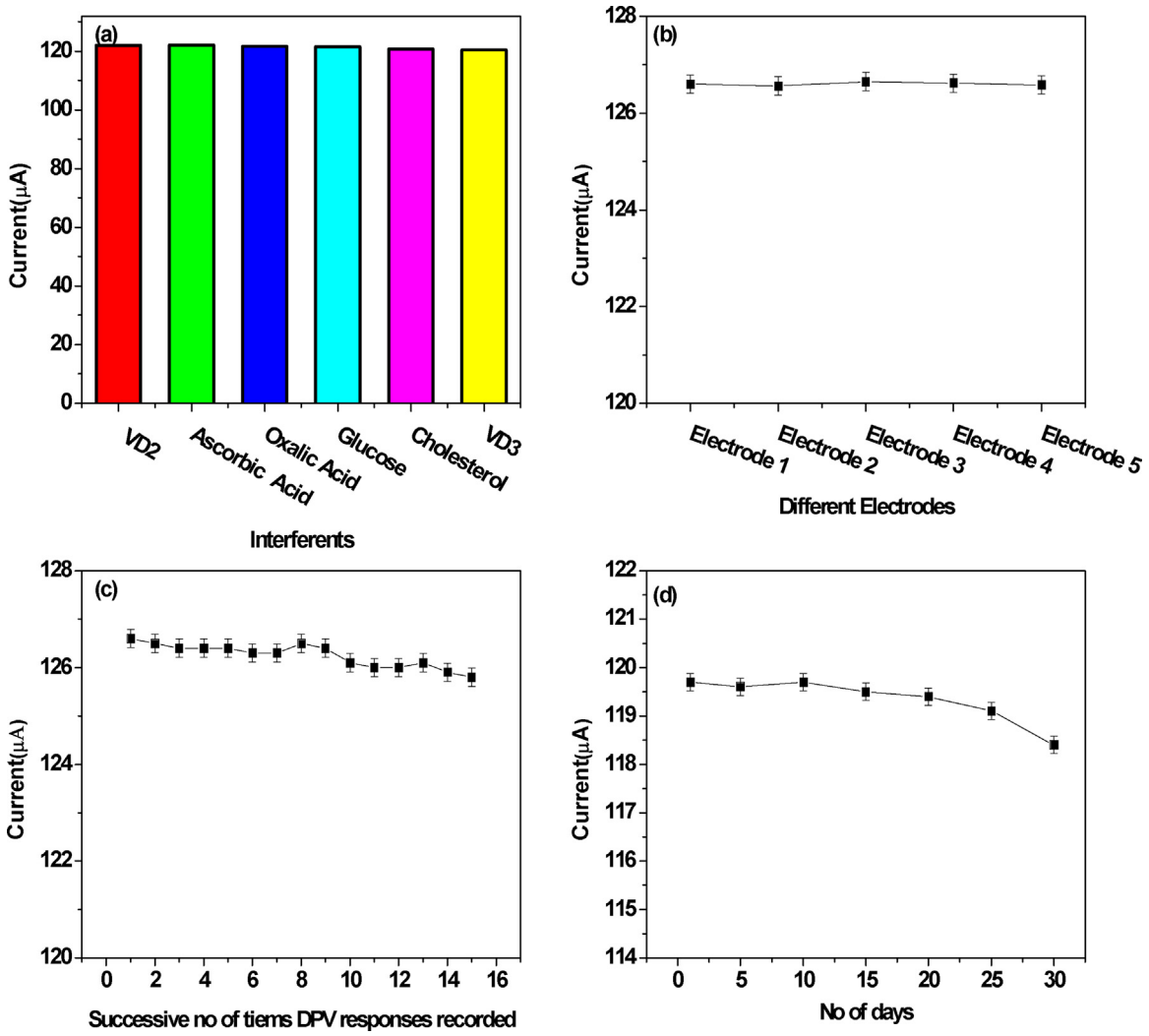


**Fig. 4.** (a) Selectivity study of BSA/Ab-$VD_2$/CD-CH/ITO bioelectrode; (b) reproducibility study of BSA/Ab-$VD_2$/CD-CH/ITO bioelectrode under similar condition; (c) repeatability study of BSA/Ab-$Vd_2$/CD-CH/ITO bioelectrode; (d) shelf-life of the BSA/Ab-$Vd_2$/CD-CH/ITO bioelectrode.

that at higher scan rate (>40 mV $s^{-1}$) $E_{pa}$ is linearly proportional to $log(\nu)$. Using Laviron theory[61] charge transfer coefficient($\alpha$) and electron transfer rate constant ($k_s$) were determined by change of peak potentials with scan rate. Using the following equation [62].

$$E_{pa} = K - 2030\frac{RT}{\alpha nF}\log(v) \quad (5)$$

$$\alpha = 2.3030\frac{RT}{nF}\frac{1}{\text{slope}} \quad (6)$$

Where F is the Faraday constant (96485.35C $mol^{-1}$), $R$ is real gas constant (8.314J $mol^{-1}$ $K^{-1}$), n = no of electron transferred (2), T is temperature (300 K). Slope of $E_{pa}$vs $log\ (\nu)$ be 0.074, charge transfer coefficient ($\alpha$) was calculated to be 0.402. The electron transfer rate constant (ks) can be evaluated using equation (7) using the constraint($\eta$) = 0, which reduces to equation (8)[63].

$$\text{Log}(k_s) = \alpha\log(1-\alpha) + (1-\alpha)\log(\alpha) - \log\left(\frac{RT}{nF\nu}\right) - \frac{\alpha(1-\alpha)nF\eta}{2.3RT} \quad (7)$$

$$k_s = (1-\alpha)\frac{nFx}{RT} \quad (8)$$

where $x$ is the intercept of the anodic potential fitted line. The $k_s$ was evaluated for BSA/Ab-$VD_2$/CD-CH/ITO bioelectrode to be 75.94 $s^{-1}$. The high value of electron transfer rate constant indicates high capability of CDs for promoting electron between Ab-$VD_2$ and electrode surface.

Electrochemical impedance spectroscopy was performed applying a small amplitude AC signal with varying frequency (0.1–$10^5$ Hz) using Frequency Response Analyzer (FRA) technique. This study was carried out to measure the impedance at the electrode-electrolyte interface. Impedance of a system was given by voltage ($V$) divided by current ($I$) passing through it, both of $V$ and $I$ are function of time ($t$).

$$Z = \frac{V(t)}{I(t)} = \frac{1}{Y} = \frac{V_0\sin(2\pi ft)}{I_0\sin(2\pi ft + \varphi)}$$

Where $Y$ is the admittance of the system, $V_o$ and $I_o$ be the amplitude of voltage and current respectively, $f$ is the frequency of the voltage, $t$ is time, $\varphi$ is the phase difference between voltage and current. Generally to model the EIS spectra Randles circuit [Fig. 2 (B-i)] is used. Randles circuit involves solution resistance ($R_s$), double layer capacitance ($C_{dl}$), charge transfer resistance ($R_{CT}$) and finally Warburg impedance ($W$). The charge which is stored at the interface is $C_1$, $R_{CT}$ is the measure of current flow of redox species at the interface, $W$ represents the impedance generated by diffusion. Complex impedance of a system is expressed through Nyquist Plot on which real part of the impedance ($Z'$) is plotted along X-axis and imaginary part ($Z''$) on the Y-axis. Nyquist plot consists of a semicircular region in high frequency region which represents a charge transfer process, followed by a straight line in low frequency region

**Table 1**
Values determined from FRA.

| Electrode | Rs(Ω) | $C_1$(μF) | $R_{CT}$(kΩ) | W(μMho) | $R_2$(Ω) | Q(μMho) |
|---|---|---|---|---|---|---|
| ITO | 65.7 | 3.03 | 1.31 | | | |
| CH/ITO | 71.6 | 1.97 | 2.25 | 70.3 | 12700 | 377 |
| CD-CH/ITO | 48.3 | 2.48 | 1.38 | 143 | 255 | 378 |
| BSA/Ab/CD-CH/ITO | 56.9 | 2.62 | 1.51 | 210 | 4550 | 461 |

which represents a mass transfer process. At high frequency the $Z''$ decreases to zero because it does not provide any impedance. At low frequency region $C_1$ provides high impedance and the current passed through the $R_{CT}$ and $R_s$ region. The value of charge transfer resistance changes whenever a surface of electrode is modified. In EIS spectra diameter of the semicircle at the high frequency is a measure of $R_{CT}$ in system. EIS spectra of (a) ITO, (b) CH/ITO, (c) CD-CH/ITO, (d) BSA/Ab-$VD_2$/CD-CH/ITO electrode in PBS containing $[Fe(CN)_6]^{3-/4-}$ were recorded [Fig. 2(A)]. Each spectrum was fitted with modified Randles circuit [Fig. 2(B-ii)] by adding a resistance ($R_2$) in parallel with constant phase element ($Q$) [64]. The value of $R_{CT}$ for each electrode was obtained as mentioned in Table 1. The very high value of $R_{CT}$ for CH/ITO (2.25 kΩ) was obtained than bare ITO (1.31 kΩ) probably due to the insulating nature of CH. For CD-CH/ITO the value of $R_{CT}$ increased to 1.38 kΩ, showing very smooth charge transfer at the interface. This enhancement was probably due the presence of free electrons in carboxyl group at the surface of the CDs. After addition of Ab-$VD_2$ and BSA onto CD-CH/ITO, the value of $R_{CT}$ slightly increased (1.51 kΩ) which confirmed the strong adsorption or immobilization of Ab-$VD_2$ on the carboxyl and amine groups present at the electrode surface and provided steric hindrance to charge transfer. The values of $R_s$, $C_1$, Warburg impedance, additional resistance $R_2$ and $Q$ for every different electrode are presented in Table 1.

### 3.3. Electrochemical response study

Differential pulse voltammetry (DPV) technique was used for the detection of Ag-$VD_2$ within a potential range −0.2 to 0.5 V, with a potential step 5 mV, pulse amplitude of 25 mV, pulse period of 50 msResponse of BSA/Ab-$VD_2$/CD-CH/ITO was recorded in the range of 1–50 ng mL$^{-1}$ of Ag-$VD_2$ in PBS containing $[Fe(CN)_6]^{3-/4-}$. First the response of bioelectrode was taken in blank, and then with various concentration of Ag-$VD_2$ (1, 10, 20, 30, 40, 50 ng mL$^{-1}$). At every increasing concentration of Ag-$VD_2$ the peak current value was increased [Fig. 3 (a)]·Ag-$VD_2$ was interacted with Ab-$VD_2$ in such a way that the magnitude of peak current increases. The peak current value was plotted against the concentration of Ag-$VD_2$ [Fig. 3(c)]. The calibration curve became linear in a concentration range (10–50 ng mL$^{-1}$) with a regression coefficient (0.983). This linearity was probably due to the interaction of Ag-$VD_2$ with adequate Ab-$VD_2$ present on the BSA/Ab-$VD_2$/CD-CH/ITO bioelectrode. The parameter obtained from the calibration plot as follows (for the range 10–50 ng mL$^{-1}$) the sensitivity was 0.2 μA ng$^{-1}$mL cm$^{-2}$, limit of detection(LOD) was 1.35 ng mL$^{-1}$. The fabricated BSA/Ab-$VD_2$/CD-CH/ITO bioelectrode showed response for lowest concentration (1 ng mL$^{-1}$) of Ag-$VD_2$ as compared to Ab-25OHD modified screen printed electrode for the detection of 25-OH vitamin D (Table 2).

To determine the affinity of binding between antigen and antibody, i.e. between Ag-$VD_2$ and BSA/Ab-$VD_2$/CD-CH/ITO, Hanes Woolf Graph was plotted between $[C]/I$vs$[C]$ (Fig. 3(d)), where $[C]$ be the concentration of Ag-$VD_2$ and $I$ be the peak current recorded in DPV response. Linearity of the Hanes Woolf plot was represented by the following equation

$$\frac{[C]}{I} = \frac{1}{I_{max}}[C] + \frac{K_d}{I_{max}} \quad (9)$$

where, $1/I_{max}$ was the inverse of the steady state current determine from slope, $K_d$ be the dissociation constant determined from the intercept of the straight line. The value of dissociation constant was calculated to be 0.15 ng mL$^{-1}$. This lower value of $K_d$ was an indication of stronger affinity between Ag-$VD_2$ towards BSA/Ab-$VD_2$/CD-CH/ITO bioelectrode.

### 3.4. Interference

To see the interference behavior responses of BSA/Ab-$VD_2$/CD-CH/ITO bioelectrode towards Ag-$VD_2$ in presence of other analytes were recorded [Fig. 4(a)]. Ascorbic acid (0.1 mM), oxalic acid (1.0 mM), glucose (4.0 mM), cholesterol (4 mM), antigen vitamin $D_3$ (30 ng mL$^{-1}$) solutions were prepared of respective concentration according to their presence in human blood. At first response of BSA/Ab-$VD_2$/CD-CH/ITO biooelectrode in presence of a fixed concentration of Ag-$VD_2$ (30 ng mL$^{-1}$) was recorded (maximum current $I_0$) through DPV in PBS containing $[Fe(CN)_6]^{3-/4-}$. Then each time different analyte (10 μL) premixed with Ag-$VD_2$ (30 ng mL$^{-1}$) were added to electrolyte and responses were recorded (maximum currents $I_1$, $I_2$, $I_3$, $I_4$, $I_5$, respectively) after 10 min of incubation time. It was seen that $I_1$, $I_2$, $I_3$, $I_4$, $I_5$were almost equal to $I_0$. Thus BSA/Ab-$VD_2$/CD-CH/ITO bioelectrode was very selective towards Ag-$VD_2$.

### 3.5. Reproducibility and repeatability

BSA/Ab-$VD_2$/CD-CH/ITO bioelectrode showed good reproducibility for Ag-$VD_2$ concentration. Responses were recorded for five individual bioelectrodes towards a fixed concentration of Ag-$VD_2$ (30 ng mL$^{-1}$). No significant change in the maximum current value was observed. The standard deviation value was obtained to be 0·3·TheBSA/Ab-$VD_2$/CD-CH/ITO also showed good repeatability characteristics as proved by the low RSD value (0.19%) till n = 5. Slight decreased observed after 5 time uses.

### 3.6. Shelf-life

The shelf-life of BSA/Ab-$Vd_2$/CD-CH/ITO bioelectrode was observed by recoding the DPV response at regular gap of 5 day for 1 month. The biooelectrode showed 0.39% response after 25days. Thus, this bioelectrode was stable for almost 25 days. The bioelectrode was kept at 4 °C while not using.

## 4. Conclusions

Vitamin $D_2$ biosensor was successfully prepared with BSA/Ab-$Vd_2$/CD-CH/ITO bioelectrode. CDs were synthesized *via* microwave pyrolysis method and dialyzed. Formations of CDs were confirmed using TEM, FTIR and UV/VIS spectroscopy. 20 μL of CDs solution was mixed with 1% chitosan (CH) solution for CD-CH composite preparation. A thin film of 30 μL of CD-CH composite was

**Table 2**
Biosensing parameters of BSA/Ab-$VD_2$/CD-CH/ITO bioelectrode as compared to previously reported.

| Bio-electrode | Detecting Antigen | Transduction | Range | LOD | Sensitivity | Ref- |
|---|---|---|---|---|---|---|
| Ab-25OHD-SPE | Ag-25OHVD | DPV | 20–200 | 10 ng/mL | 0.2 μA ng$^{-1}$ mL cm$^{-2}$ | [53] |
| BSA/Ab/CD-CH/ITO. | Ag-VD2 | DPV | 1–50 | 1.35 ng/mL | 0.02 μA ng$^{-1}$ mL | Present Study |

drop casted onto ITO surface. The surface wettability and roughness of CD-CH/ITO electrode was characterized by static contact angle measurements and AFM study, respectively. Ab-$VD_2$ was immobilized *via* EDC-NHS coupling and further BSA was used a blocking agent immobilized. The oxidation and reduction of this prepared BSA/Ab-$VD_2$/CD-CH/ITO bioelectrode was observed by cyclic voltammogram. The impedance at the bioelectrode-electrolyte interface was measured by FRA technique. The response of BSA/Ab-$Vd_2$/CD-CH/ITO bioelectrode with respect to different concentrations of Ag-$VD_2$ (1–50 ng $mL^{-1}$) was recorded using DPV technique. Linearity was observed between 10 and 50 ng $mL^{-1}$ of Ag-$VD_2$ concentration with sensitivity 0.2 μA $ng^{-1}$ mL $cm^{-2}$ and LOD was found out to be 1.35 ng $mL^{-1}$. This biosensor was very specific to vitamin $D_2$ and has a shelf-life of over 25 days. Efforts to be made to improve the LOD value of D2 biosensing platform for detection of D2 concentration in milk shakes or other samples.

## Acknowledgements:

Authors thank to AIRF, JNU for allowing using TEM, FTIR. TS acknowledge the University Grant Commission, India for granting fellowship. Authors thank to Prof. Subhasis Ghosh, School of Physical Sciences, JNU for allowing access to AFM studies. The authors want to thank Department of Science & Technology (DST- Purse and DST Nanomission), Department of Biotechnology, New Delhi and University Grants Commission (UPE-II, Project-58), India for funding for the project.

## References

[1] S.N. Baker, G.A. Baker, Angew. Chem. Int. Ed. 49 (2010) 6726–6744.
[2] H. Liu, T. Ye, C. Mao, Angew. Chem. Int. Ed. 46 (2007) 6473–6475.
[3] X. Zhai, P. Zhang, C. Liu, T. Bai, W. Li, L. Dai, W. Liu, Chem. Commun. 48 (2012) 7955–7957.
[4] J. Wang, C.F. Wang, S. Chen, Angewandte Chemie 124 (2012) 9431–9435.
[5] Q.L. Zhao, Z.L. Zhang, B.H. Huang, J. Peng, M. Zhang, D.W. Pang, Chem. Commun. (2008) 5116–5118.
[6] S. Sahu, B. Behera, T.K. Maiti, S. Mohapatra, Chem. Commun. 48 (2012) 8835–8837.
[7] C. Zhu, J. Zhai, S. Dong, Chem. Commun. 48 (2012) 9367–9369.
[8] M. Sheng, Y. Gao, J. Sun, F. Gao, Biosens. Bioelectron. 58 (2014) 351–358.
[9] L. Cao, X. Wang, M.J. Meziani, F. Lu, H. Wang, P.G. Luo, Y. Lin, B.A. Harruff, L.M. Veca, D. Murray, J. Am. Chem. Soc. 129 (2007) 11318–11319.
[10] W. Shi, Q. Wang, Y. Long, Z. Cheng, S. Chen, H. Zheng, Y. Huang, Chem. Commun. 47 (2011) 6695–6697.
[11] Z. Lin, W. Xue, H. Chen, J.-M. Lin, Anal. Chem. 83 (2011) 8245–8251.
[12] S. Liu, J. Tian, L. Wang, Y. Zhang, X. Qin, Y. Luo, A.M. Asiri, A.O. Al-Youbi, X. Sun, Adv. Mater. 24 (2012) 2037–2041.
[13] W. Lu, X. Qin, S. Liu, G. Chang, Y. Zhang, Y. Luo, A.M. Asiri, A.O. Al-Youbi, X. Sun, Anal. Chem. 84 (2012) 5351–5357.
[14] C. Liu, P. Zhang, X. Zhai, F. Tian, W. Li, J. Yang, Y. Liu, H. Wang, W. Wang, W. Liu, Biomaterials 33 (2012) 3604–3613.
[15] X. Huang, L. Yang, S. Hao, B. Zheng, L. Yan, F. Qu, A.M. Asiri, X. Sun, Inorg. Chem. Front. 4 (2017) 537–540.
[16] H. Zhu, X. Wang, Y. Li, Z. Wang, F. Yang, X. Yang, Chem. Commun. (2009) 5118–5120.
[17] Y. Dong, R. Wang, H. Li, J. Shao, Y. Chi, X. Lin, G. Chen, Carbon 50 (2012) 2810–2815.
[18] K. Wang, Q. Liu, L. Dai, J. Yan, C. Ju, B. Qiu, X. Wu, Anal. Chim. Acta 695 (2011) 84–88.
[19] Y. Li, Y. Hu, Y. Zhao, G. Shi, L. Deng, Y. Hou, L. Qu, Adv. Mater. 23 (2011) 776–780.
[20] L. Cao, S. Sahu, P. Anilkumar, C.E. Bunker, J. Xu, K.S. Fernando, P. Wang, E.A. Guliants, K.N. Tackett, Y.-P. Sun, J. Am. Chem. Soc. 133 (2011) 4754–4757.
[21] Y.P. Sun, B. Zhou, Y. Lin, W. Wang, K.S. Fernando, P. Pathak, M.J. Meziani, B.A. Harruff, X. Wang, H. Wang, J. Am. Chem. Soc. 128 (2006) 7756–7757.
[22] X. Xu, R. Ray, Y. Gu, H.J. Ploehn, L. Gearheart, K. Raker, W.A. Scrivens, J. Am. Chem. Soc. 126 (2004) 12736–12737.
[23] L. Tian, D. Ghosh, W. Chen, S. Pradhan, X. Chang, S. Chen, Chem. Mater. 21 (2009) 2803–2809.
[24] Y. Dong, N. Zhou, X. Lin, J. Lin, Y. Chi, G. Chen, Chem. Mater. 22 (2010) 5895–5899.
[25] Y. Li, Y. Zhao, H. Cheng, Y. Hu, G. Shi, L. Dai, L. Qu, J. Am. Chem. Soc. 134 (2011) 15–18.
[26] J. Lu, J. Yang, J. Wang, A. Lim, S. Wang, K. Loh, CrossRef| PubMed| CAS| Web of Science® Times Cited 64 (2011).
[27] A. Jaiswal, S.S. Ghosh, A. Chattopadhyay, Chem. Commun. 48 (2012) 407–409.
[28] Z. Lin, W. Xue, H. Chen, J.-M. Lin, Chem. Commun. 48 (2012) 1051–1053.
[29] S. Zhang, Q. Pu, P. Liu, Q. Sun, Z. Su, Anal. Chim. Acta 452 (2002) 223–230.
[30] P.R. Solanki, M.K. Patel, M.A. Ali, B. Malhotra, J. Mater. Chem. B 3 (2015) 6698–6708.
[31] M.G. Peter, J. Macromol. Sci. Part A: Pure Appl. Chem. 32 (1995) 629–640.
[32] S. Hudson, C. Smith, Polysaccharides: chitin and chitosan: chemistry and technology of their use as structural materials, in: Biopolymers from Renewable Resources, Springer, 1998, pp. 96–118.
[33] R.N. Tharanathan, F.S. Kittur, (2003).
[34] K. Kurita, Prog. Polym. Sci. 26 (2001) 1921–1971.
[35] C. Peniche, W. Argüelles-Monal, H. Peniche, N. Acosta, Macromol. Biosci. 3 (2003) 511–520.
[36] I.R.W.Z. de Oliveira, I.C. Vieira, Enzyme Microb. Technol. 38 (2006) 449–456.
[37] M. Zhang, A. Smith, W. Gorski, Anal. Chem. 76 (2004) 5045–5050.
[38] X. Lu, J. Hu, X. Yao, Z. Wang, J. Li, Biomacromolecules 7 (2006) 975–980.
[39] Q. Huang, S. Hu, H. Zhang, J. Chen, Y. He, F. Li, W. Weng, J. Ni, X. Bao, Y. Lin, Analyst 138 (2013) 5417–5423.
[40] Q. Huang, H. Zhang, S. Hu, F. Li, W. Weng, J. Chen, Q. Wang, Y. He, W. Zhang, X. Bao, Biosens. Bioelectron. 52 (2014) 277–280.
[41] M.F. Holick, New Engl. J. Med. 357 (2007) 266–281.
[42] M.F. Holick, J. Clin. Invest. 116 (2006) 2062–2072.
[43] R. Bouillon, L. De Groot, J. Jameson, (2001).
[44] M. Del Carlo, A. Pepe, M. Sergi, M. Mascini, A. Tarentini, D. Compagnone, Talanta 81 (2010) 76–81.
[45] H.F. DeLuca, Am. J. Clin. Nutr. 80 (2004) 1689S–1696S.
[46] H.M. Trang, D. Cole, L.A. Rubin, A. Pierratos, S. Siu, R. Vieth, Am. J. Clin. Nutr. 68 (1998) 854–858.
[47] L.A. Armas, B.W. Hollis, R.P. Heaney, J. Clin. Endocrinol. Metabol. 89 (2004) 5387–5391.
[48] M.F. Holick, R.M. Biancuzzo, T.C. Chen, E.K. Klein, A. Young, D. Bibuld, R. Reitz, W. Salameh, A. Ameri, A.D. Tannenbaum, J. Clin. Endocrinol. Metabol. 93 (2008) 677–681.
[49] L. Jafri, A.H. Khan, A.A. Siddiqui, S. Mushtaq, R. Iqbal, F. Ghani, I. Siddiqui, Clin. Biochem. 44 (2011) 864–868.
[50] G. Snellman, H. Melhus, R. Gedeborg, L. Byberg, L. Berglund, L. Wernroth, K. Michaelsson, PLoS One 5 (2010) e11555.
[51] H.J. Roth, H. Schmidt-Gayk, H. Weber, C. Niederau, Ann. Clin. Biochem. 45 (2008) 153–159.
[52] G.L. Lensmeyer, D.A. Wiebe, N. Binkley, M.K. Drezner, Clin. Chem. 52 (2006) 1120–1126.
[53] L. Carlucci, G. Favero, C. Tortolini, M. Di Fusco, E. Romagnoli, S. Minisola, F. Mazzei, Biosens. Bioelectron. 40 (2013) 350–355.
[54] S.K. Vashist, Diagnostics 2 (2012) 23–33.
[55] K. Nagaraju, R. Reddy, N. Reddy, J. Appl. Biomater. Funct. Mater. 13 (2015).
[56] H. Ding, L.-W. Cheng, Y.-Y. Ma, J.-L. Kong, H.-M. Xiong, New J. Chem. 37 (2013) 2515–2520.
[57] S. Zhu, Q. Meng, L. Wang, J. Zhang, Y. Song, H. Jin, K. Zhang, H. Sun, H. Wang, B. Yang, Angew. Chem. Int. Ed. 52 (2013) 3953–3957.
[58] A. Salinas-Castillo, M. Ariza-Avidad, C. Pritz, M. Camprubí-Robles, B. Fernández, M.J. Ruedas-Rama, A. Megia-Fernández, A. Lapresta-Fernández, F. Santoyo-Gonzalez, A. Schrott-Fischer, Chem. Commun. 49 (2013) 1103–1105.
[59] B. Yin, J. Deng, X. Peng, Q. Long, J. Zhao, Q. Lu, Q. Chen, H. Li, H. Tang, Y. Zhang, Analyst 138 (2013) 6551–6557.
[60] H. Li, X. He, Y. Liu, H. Huang, S. Lian, S.-T. Lee, Z. Kang, Carbon 49 (2011) 605–609.
[61] E. Laviron, J. Electroanal. Chem. Interfacial Electrochem. 101 (1979) 19–28.
[62] A. Salimi, L. Miranzadeh, R. Hallaj, Talanta 75 (2008) 147–156.
[63] A.L. Eckermann, D.J. Feld, J.A. Shaw, T.J. Meade, Coord. Chem. Rev. 254 (2010) 1769–1802.
[64] T. Sarkar, K. Rawat, H. Bohidar, P.R. Solanki, J. Electroanal. Chem. 783 (2016) 208–216.